


ORIGINAL ARTICLE

Soil macroporosity and water flow in the root zone of oases in hyper-arid regions

Yongyong Zhang^{1,2}  | Angyuan Jia³ | Wenzhi Zhao^{1,2} | Jianjun Kang^{1,2} | Chuan Wang^{1,2} | Wenrong Kang^{1,2} | Zihan Tian^{1,2}

¹Linze Inland River Basin Research Station, Key Laboratory of Ecohydrology of Inland River Basin, Northwest Institute of Eco-Environment and Resources, Chinese Academy of Sciences, Lanzhou, China

²University of Chinese Academy of Sciences, Beijing, China

³National Engineering Laboratory for Improving Quality of Arable Land, Institute of Agricultural Resources and Regional Planning, Chinese Academy of Agricultural Sciences, Beijing, China

Correspondence

Yongyong Zhang, Linze Inland River Basin Research Station, Key Laboratory of Ecohydrology of Inland River Basin, Northwest Institute of Eco-Environment and Resources, Chinese Academy of Sciences, Lanzhou 730000, China.
Email: zhangyongyong@lzb.ac.cn

Funding information

National Natural Science Foundation of China, Grant/Award Numbers: 41877153, 42071044; Youth Innovation Promotion Association of the Chinese Academy of Sciences, Grant/Award Number: 2020420

Abstract

The characteristics of soil macropores and water infiltration are closely connected to the growth of plant roots and their root zone environment. However, it is unclear how the root zone environment of oasis farmlands regulates the development of soil macropores and water flow in hyper-arid regions. The objective of this study was to investigate soil macropores and their effect on water flow under irrigated oasis farmlands using a combination of X-ray computed tomography (CT) and dye tracer. It was hypothesized that the integration of CT and dye tracer could clearly reveal preferential flow through biopores and large pores of oasis soils. A helical medical CT scanner was used to quantify more information about soil macropores in the root zone, along with an in situ single-ring dye infiltration experiment to reveal water flow in three different oasis farmlands (piedmont oasis farmland, marginal oasis farmland, and old oasis farmland). Soil macroporosity was 0.44% under crop rows, while soil macroporosity in the interrows was only 0.30% across the oasis farmlands. Biopores contributed 73% of the volume of the total macropores under crop rows. The stable infiltration rate in the interrows was 0.3 mm min^{-1} , which was significantly ($p < 0.05$) less than that under crop rows (0.7 mm min^{-1}). Water flow under crop rows were mainly transported in biopores and large pores. The contribution of macropores to preferential flow under crop rows was 4.8 times larger than interrows. The integration of CT and dye tracer was a more holistic technique, which adequately revealed that oases had preferential flow affected by biopores and large pores, resulting in higher solute and contaminant transport.

KEYWORDS

dye tracer, preferential flow, soil structure, water infiltration, X-ray tomography

Key Points

- Soil macropores and preferential flow affected by crop roots were investigated in hyper-arid regions.
- The integration of CT and dye tracer adequately identified preferential flowpaths of oasis soils.

- Biopores were larger under crop rows than interrows.
- Preferential flow transported in biopores and large soil pores under crop rows.

1 | INTRODUCTION

Soil water infiltration is an important hydrological process that links surface water and groundwater (Wang et al., 2008; Zhang et al., 2019). Infiltration process varies among land use types and influences soil water movement and soil water distribution. Decayed roots provide preferential downward pathways for water to infiltrate the soil, influencing solute migration and contaminant transport (Backnäs et al., 2012; Nimmo, 2021), improving soil permeability, and influencing soil water distribution in different land use types (Hendrickx & Flury, 2001; Jarvis, 2020). As indirectly inferred by the related studies, root-mediated water flow might have a profound impact on the exchange of surface water and groundwater in arid regions (Li et al., 2013; Liu et al., 2020; Zhang et al., 2021).

Oasis farmlands in hyper-arid regions of China are an important area for grain production. The healthy and sustainable development of oasis agriculture is vitally important to maintain the stability of the desert-oasis ecosystems. However, water shortage has become an important factor restricting agricultural development of oases. Agricultural irrigation water accounts for 90% of the total water consumption in the desert-oasis regions (Kang et al., 2017). Better understanding of soil water movement in oasis farmlands would help guide agricultural irrigation in arid areas (Zhang et al., 2019). There are many factors including soil properties (bulk density, soil organic carbon, soil texture, and soil aggregates), irrigation technique, tillage method, and biological factors, that affect soil water infiltration (Koestel et al., 2012; Koestel & Jorda, 2014; Lipiec et al., 2006). Among these factors, plant roots significantly affect soil water infiltration in arid areas (Devitt & Smith, 2002; Wu et al., 2017). Therefore, it is necessary to explore and characterise more information about soil macropores created by plant roots and their effect on the extent of preferential flow in hyper-arid regions.

X-ray computed tomography (CT) has been widely used to quantitatively analyse the three-dimensional structure of soil macropore networks (Li et al., 2019; Luo et al., 2010; Zhang et al., 2017). Macropores are large soil voids and pathways, for example, root channels, and connected large pores can permit preferential flow through the soil profile (Hendrickx & Flury, 2001; Jarvis, 2020). The CT method provided more information about the

characteristics and continuity of macropores (Filipović et al., 2020). Lucas et al. (2019) used the CT method to visualise soil pore architecture affected by plant roots. Soil pore features obtained by CT are expected to study preferential flow and solute transport within the soil profile. However, the adoption of CT alone is not sufficient to reveal water flow and solute transport processes in large soil pores. In addition, in situ dye tracer experiments and site measurements are most used to trace water flow patterns (Kodešová et al., 2012; Mooney & Morris, 2008). The studies on preferential flow affected by plant roots using the dye tracer method mainly focused on forest and cropland ecosystems (Benegas et al., 2014; Jiang et al., 2018). However, the dye tracer is a destructive method when detecting preferential flow patterns (Zhang, Zhao, et al., 2018). Thus, the best way is to integrate different methods, which could overcome some of the short comings of individual method.

Plant roots influence the morphological characteristics of soil macropores (Guo et al., 2020; Noguchi et al., 1997). The growth and extension of the root system increase the macroporosity of soil profile. Heterogeneity in plant root architecture causes variation in soil macropore structure. For example, horizontal roots created macropores of the shallow soil, and the presence of vertical roots and oblique roots created macropores of the deeper soil layers (Li et al., 2013, 2019). Root systems were associated with 70% of soil macropores in top soil (Cheng et al., 2011). In addition, the turnover of plant roots increases soil organic matter and water-stable aggregates, enhancing soil infiltration (Bargués Tobella et al., 2014; Bogner et al., 2008). For example, the root system increases infiltration capacity compared to soils lacking roots (Li et al., 2013). In a semi-arid watershed (Extremadura, Spain), infiltration rate was significantly correlated with root channels (van Schaik, 2009). However, the biomass of roots is relatively low, and the turnover of roots is slow in hyper-arid regions (Lai et al., 2016; Li et al., 2013; Zhang et al., 2021). In fact, the mechanisms of soil macropores and water flow regulated by the root zone environment have not been investigated in oasis farmlands.

The macropores and their flow pathways would be active when the soil is close to saturation (Beven & Germann, 1982; Jarvis, 2020). In arid regions, preferential flow could occur when the large pores are active mostly because of rapid moistening by irrigation. In our study, it was hypothesized that the integration of CT and dye

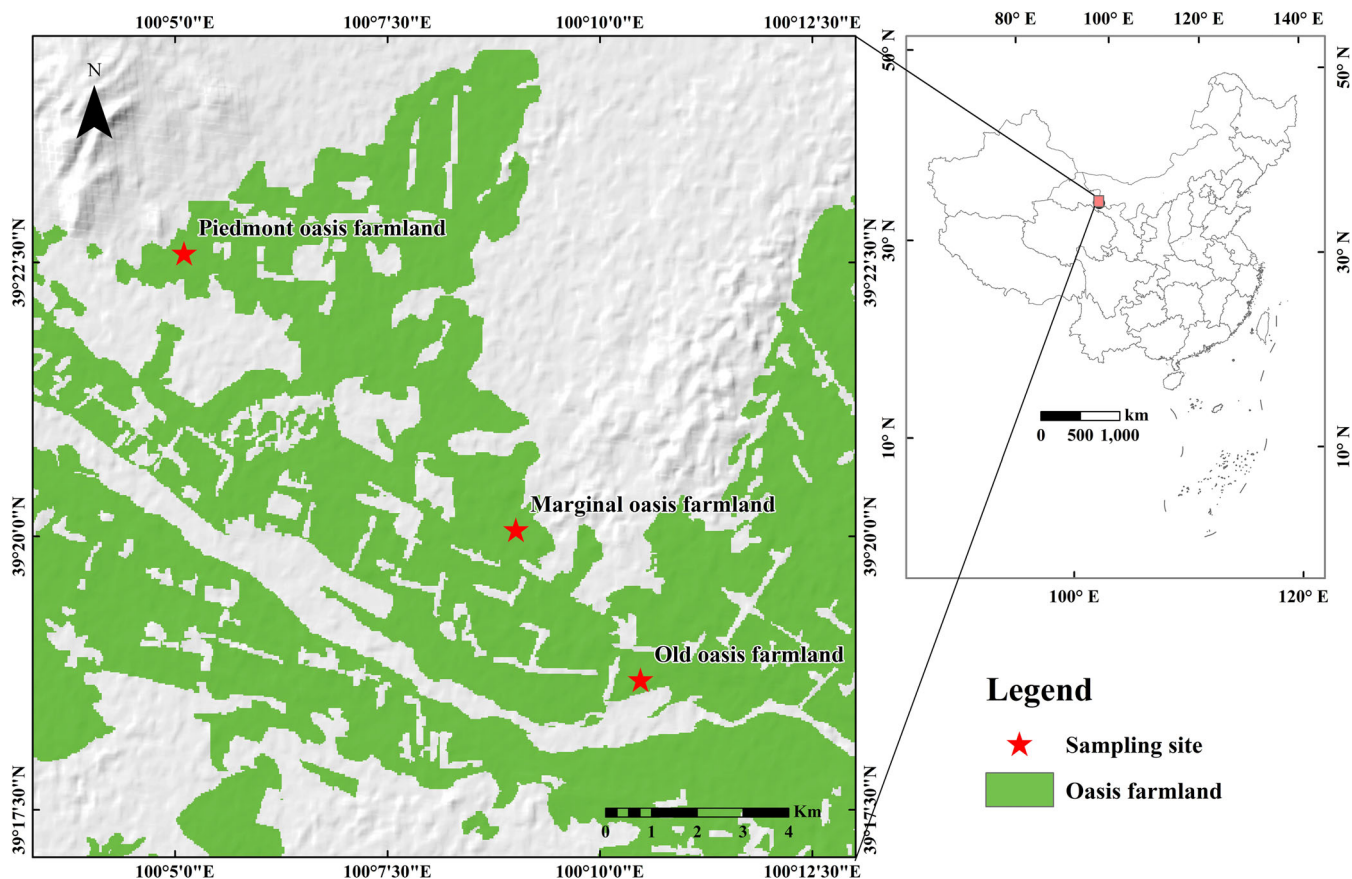


FIGURE 1 Location of the study area

tracer could clearly reveal preferential flow through biopores and large pores in oasis farmlands. We not only used CT to quantify soil macropore characteristics, but also combined an in situ single-ring dye infiltration experiment to quantify infiltration characteristics affected by the root zone. The aims of this study were (i) to quantify the influence of the root zone on soil macropore architectures, and (ii) to combine CT and dye tracer to visualise the effect of soil macropores on preferential flow patterns in oases of hyper-arid regions.

2 | MATERIALS AND METHODS

2.1 | Study site description

The study area was located in the middle of Heihe River of Northwest China ($99^{\circ}51' - 100^{\circ}30'E$, $38^{\circ}57' - 39^{\circ}42'N$, Altitude: 1374 m, Figure 1). The region is a typical arid desert climate, with an annual average precipitation of about 120 mm and mean pan evaporation of about $2380 \text{ mm year}^{-1}$. The precipitation from July to September accounts for about 60% of the total annual precipitation (Zhang et al., 2019). In the last 20 years, the annual average temperature was 7.6°C .

The annual average sunshine duration is 3051 h. Annual average wind speed is 3.2 m/s. The main landscape types in the study area are farmlands in oasis region and shrublands in desert region (Zhang et al., 2021). The irrigated farmlands are distributed along the middle reaches of Heihe River.

Three types of oasis farmland (old oasis farmland, marginal oasis farmland, and piedmont oasis farmland) were determined as the study sites (Figure 1). The newly reclaimed marginal oasis farmland (MOF) close to semi-desert shrubs has low soil organic carbon content, low soil water retention, and low soil fertility. The old oasis farmland (OOF) has been tilled nearly 100 years ago and has better soil quality due to long-term fertilisation and irrigation (Zhang, Zhao, et al., 2018). The piedmont oasis farmland (POF) was deposited by mountain floods with silt-laden water and reclaimed to farmland. Ridge tillage has been commonly adopted here. The major crop in the three types of oasis farmlands was maize grown with furrow irrigation. In order to reuse mulched plastic film under crop rows, crop lines were fixed, and the selected all oasis farmlands were not tilled in 2019 and 2020. The row spacing was 40–50 cm. Maize was harvested in September. The experiments were conducted after harvesting in 2020.

2.2 | Soil sampling and soil physical properties

Soil sampling was conducted in the three types of oasis farmlands in October. At each oasis farmland, three randomly replicated soil samples were taken at intervals of 10 cm from 0 to 30 cm soil depth and homogenised for subsequent analysis of soil properties. Soil texture was analysed with a laser analyser Mastersizer 2000 (Eshel et al., 2004). The undisturbed soil under crop rows and interrows at each oasis farmland were sampled using a soil sampler with a 5 cm diameter and 5 cm high stainless steel cutting ring, respectively. The bulk density was determined using the thermogravimetric method (Zhang, Zhao, et al., 2018). Soil samples for measuring soil organic matter were taken under crop rows and interrows at each oasis farmland, respectively. Soil organic matter was measured by oven heating weighed soil samples at 400°C for 12 h (Heiri et al., 2001) then reweighing the samples to calculate the fraction of soil organic matter. The procedure is called “loss on ignition” since the organic matter is burned off during the process (Davies, 1974), which removed most of the soil organic matter from the soil samples (Heiri et al., 2001). The values of soil organic matter were validated based on the measurements using the dichromate oxidation method in the study areas (Zhang et al., 2017, 2021).

2.3 | Soil column sampling, scanning, and image analysis

To investigate the characteristics of three-dimensional soil macropore networks, we used polyvinyl chloride (PVC) pipes (20 cm in diameter, 30 cm in height) to collect undisturbed soil columns from 0 to 30 cm depth in the three types of oasis farmlands. At each oasis farmland, three random replicates were collected under crop rows and three replicates from interrows, respectively, resulting in a total of 18 soil columns. Soil columns were vertically peeled using knives. To prevent any disturbances, the PVC cylinders were gently inserted vertically from the top to 30 cm depth. To avoid evaporation, the soil columns were carefully wrapped with plastic film immediately after sampling. The CT scanner (Optima CT520, GE, USA) located at Linze County People's Hospital was used to scan soil columns. The excitation voltage and current were 100 kV and 100 mA, respectively. Voxel size of the scanned images was 0.469 mm × 0.469 mm × 0.625 mm. The CT scanning generated 480 digital slices for each soil column. 20 images from the top of soil column and 20 images in the each soil bottom were discarded to

remove edge effects. A resulting 440 images were used to analyse soil pore architectures. Thus, the height of the region of interest inside soil column was 275 mm.

The software ImageJ (ver.1.50e, NIH, USA) was used to visualise three-dimensional soil macropore networks. To reduce the effect of inevitable disturbance along the inner edge of soil columns, a square (120 mm × 120 mm) was selected in the centre of each image for visualising soil macropores. A maximum entropy segmentation algorithm was initially used for image binarization. Then, the threshold value was visually adjusted by comparing the binary images with the original greyscale images of the CT scanning (Schindelin et al., 2012). The ImageJ plug-in 3D Viewer was used to visualise the three-dimensional structure of soil macropores (Schindelin et al., 2012). The macropore number, macropore surface area (cm²), and macropore volume (mm³) were obtained using the ImageJ plug-in 3D Object Count (Zhang et al., 2017). In order to describe the structure of biopores, tubular pores from the macropore networks were segmented (Lucas et al., 2019). To do so, the Fiji software plug-in Tubeness was used to detect the biopores (Schindelin et al., 2012), which has been developed for blood vessel detection (Frangi et al., 1998). The fractal dimensions were obtained using the ImageJ plug-in Bone-J (Doubé et al., 2010). The macropore diameter (MD) was calculated as:

$$MD = 2\sqrt{AM/\pi}, \quad (1)$$

where AM is the area of each two-dimensional slice.

2.4 | Soil infiltration experiment, dye tracer experiment, and dye imaging process

An in situ single-ring dye infiltration experiment was placed 1 m away from each collected soil column. A total of 18 infiltration measurements with three replicates per farmland type were performed under crop rows and interrows, respectively. A ring with 20 cm diameter was gently pushed into the soil to 20 cm depth. The soil walls around the inner and outer sides of the ring were compacted to avoid lateral flow outside the ring. A 4 g L⁻¹ solution of Brilliant Blue FCF was irrigated during the experiments (Zhang, Zhao, et al., 2018). The water head in the ring was kept constant at 5 cm using Mariotte flask, and the supplying water volume was 100 mm at each site based on actual furrow irrigation in fields. The water level in the Mariotte flask was recorded every 3 min at the beginning of the experiment and every 10 min after 30 min. The infiltration rate was estimated during the dye tracer experiment.

After 48 h, the soil profile was excavated vertically along the diameter of the ring. According to the actual infiltration depth, soil profiles were dug to a depth of 50 cm and a width of 20 cm. The stained vertical profiles (20 cm width and 50 cm depth) were photographed using a Canon D-60 digital camera (5184 pixel \times 3456 pixel). To avoid direct sunlight, a shade umbrella was used to cover the soil pits during photographing. The dye staining characteristics of each soil profile were obtained.

The dye staining image of the soil profile was cropped and geometrically corrected using Photoshop software (ver. CS6, Adobe, USA). The processed image was then manually binarized in ImageJ software (ver.1.50e, NIH, USA). We used the ArcMap10 plug-in Tabulate area tool to calculate the soil staining characteristics (dye coverage, uniform infiltration depth, maximum infiltration depth [MID], length index of preferential flow, and preferential flow fraction). The dye coverage refers to the ratio of the soil dye area to the entire section area. Uniform infiltration depth (UID) is interpreted as the depth at which dye coverage decreases below 80%, which represents the depth of the uniform infiltration front where the infiltration process is dominated by uniform flow (van Schaik, 2009). Length index (LI) of preferential flow refers to the absolute difference between the upper and lower dyed areas per unit soil depth of the soil dye profile. LI represents the degree of heterogeneity of the dye staining flow patterns, which is calculated as follows (Bargués Tobella et al., 2014):

$$LI = \sum_{i=1}^n |D_{i+1} - D_i|, \quad (2)$$

where the dye staining area is divided into n layers, D_i represents the dye staining area of i layer.

Preferential flow fraction (PFF) is described as the fraction of total infiltration that flows through the

preferential flow pathways. Soils with a high degree of preferential flow fraction will have high value. The calculation formula of PFF is as follows (Bargués Tobella et al., 2014):

$$PFF = \left(1 - \frac{UID * W}{D}\right) \times 100, \quad (3)$$

where UID is the uniform infiltration depth (cm), W is the width of soil profile (20 cm), and D is the dye coverage area (cm²).

2.5 | Statistical analysis

Statistical analysis was performed using the software program SPSS, ver. 21.0 (SPSS Inc., Chicago, IL, USA). All data with three replicates were expressed as the mean values \pm standard deviation. Significant differences were evaluated at the 0.05 probability level. A Kruskal-Wallis test ($p < 0.05$) was used to compare soil macropore characteristics and water flow indices between crop rows and interrows. Spearman's correlation coefficients were used to analyse the relationships between soil macropore characteristics and preferential flow indices across the oasis farmlands.

3 | RESULTS

3.1 | Soil properties

A variance of soil particle size distribution was observed among the three types of oasis farmlands (Table 1). Soils of the oasis farmlands differed in sand content, with the highest average value in MOF (82.1%), followed by OOF (62.0%) and POF (25.4%). According to the United States Department of Agriculture (USDA) classification system,

TABLE 1 Soil properties in the three types of oasis farmlands

| Sites | Depth (cm) | Particle size distribution (%) | | | Bulk density (g/cm ³) | | Soil organic matter (g/kg) | |
|-------------------------------|------------|--------------------------------|----------------------|------------------|-----------------------------------|-----------------|----------------------------|------------------|
| | | Sand (0.05–2.00 mm) | Silt (0.002–0.05 mm) | Clay (<0.002 mm) | Interrow | Crop row | Interrow | Crop row |
| Piedmont oasis farmland (POF) | 0–30 | 25.4 \pm 3.2 c | 62.1 \pm 2.7 a | 12.5 \pm 1.3 a | 1.55 \pm 0.03 | 1.50 \pm 0.02 | 20.0 \pm 2.1 b | 27.0 \pm 1.9 a |
| Old oasis farmland (OOF) | 0–30 | 62.0 \pm 1.9 b | 32.3 \pm 1.2 b | 5.6 \pm 0.8 b | 1.48 \pm 0.03 | 1.44 \pm 0.02 | 16.0 \pm 2.0 b | 21.1 \pm 3.1 a |
| Marginal oasis farmland (MOF) | 0–30 | 82.1 \pm 2.1 a | 14.6 \pm 1.9 c | 3.3 \pm 0.3 b | 1.51 \pm 0.03 | 1.45 \pm 0.03 | 13.0 \pm 2.0 b | 20.2 \pm 1.8 a |

Note: Values represent means followed by the standard deviation. Different letters mean significant difference at 0.05 level.

MOF was classified as sandy soil, OOF as loamy sand, and POF as silt clay loam. Soils under crop rows had lower bulk density than interrows across the oasis farmlands, but did not differ significantly ($p > 0.05$) between interrows and crop rows (Table 1). Soils under crop rows were banked up and crop roots enhanced total soil porosity. Soils under crop rows had significantly ($p < 0.05$) larger soil organic matter than interrows across the oasis farmlands (Table 1).

3.2 | Soil macropore characteristics

Soils under crop rows had more macropores than interrows across the oasis farmlands (Figure 2). In the interrows, there were more random and less continuously

distributed macropores distributed from 0 to 20 cm soil depth, which were likely soil cracks and large soil pores (Figure 2). Under crop rows, a large number of long continuously tubular pores including large root channels were observed from 0 to 20 cm depth in soil columns (Figure 3). Large pores were also distributed to some extent in the 20–30 cm soil layer under crop rows (Figure 2). Biopores and large pores were enhanced under the influence of root zone, which might lead to better pore continuity under crop rows.

The average soil macroporosity in the interrows was 0.30% across the oasis farmlands. Soil macroporosity under crop rows averaged 0.44% across the oasis farmlands, which was 1.5 times larger than interrows (Table 2). Macropore number in soils under crop rows were significantly ($p < 0.05$) larger than interrows: the

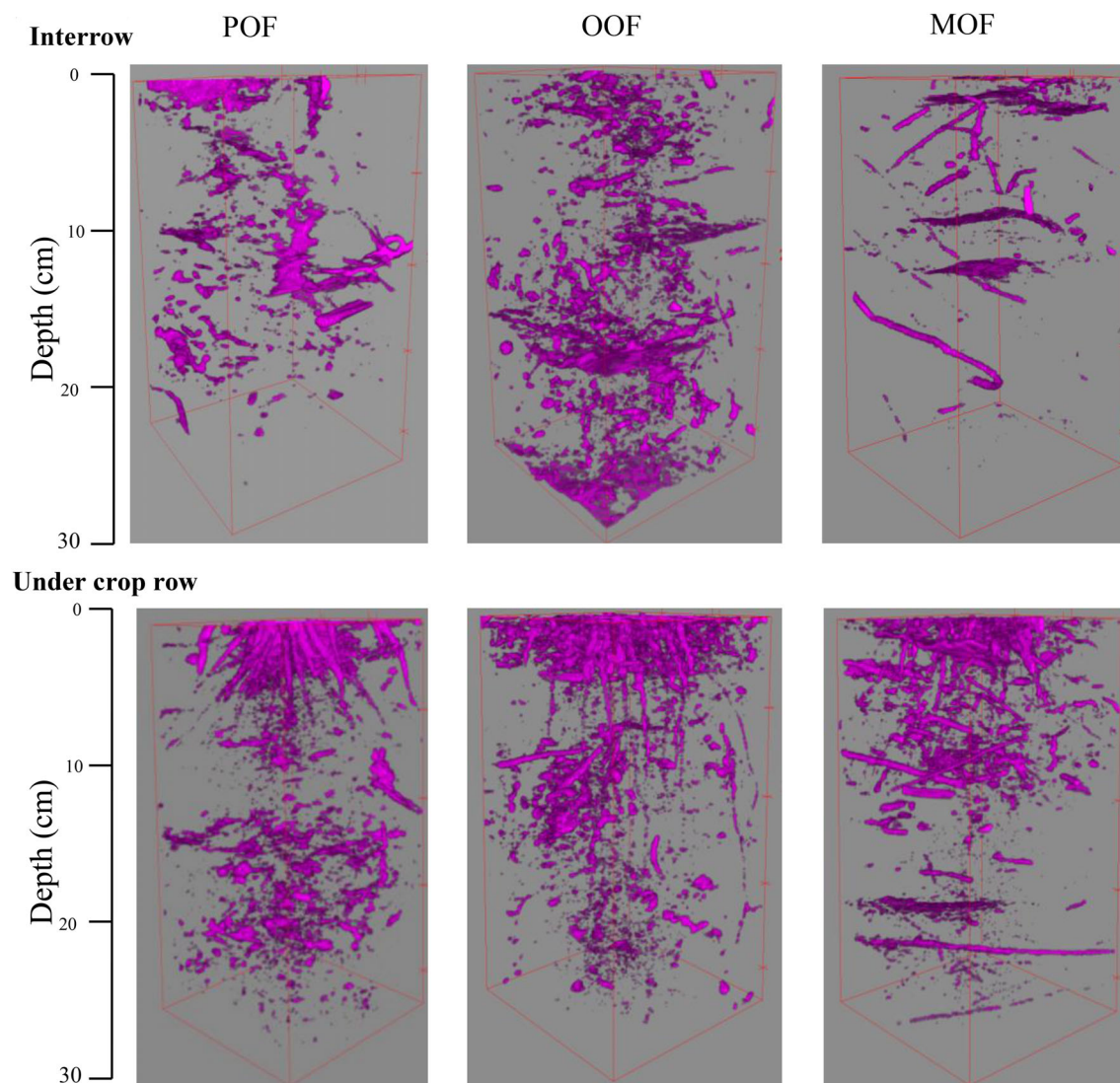


FIGURE 2 Three-dimensional soil macropore structure in the three types of oasis farmlands. POF is piedmont oasis farmland; OOF is old oasis farmland; MOF is marginal oasis farmland. The dimension of the region of interest is 12 cm × 12 cm × 27.5 cm for each soil core column. Top: Three-dimensional soil macropore structure in the interrows of three types of farmlands; bottom: Three-dimensional soil macropore structure under crop rows of three types of farmlands

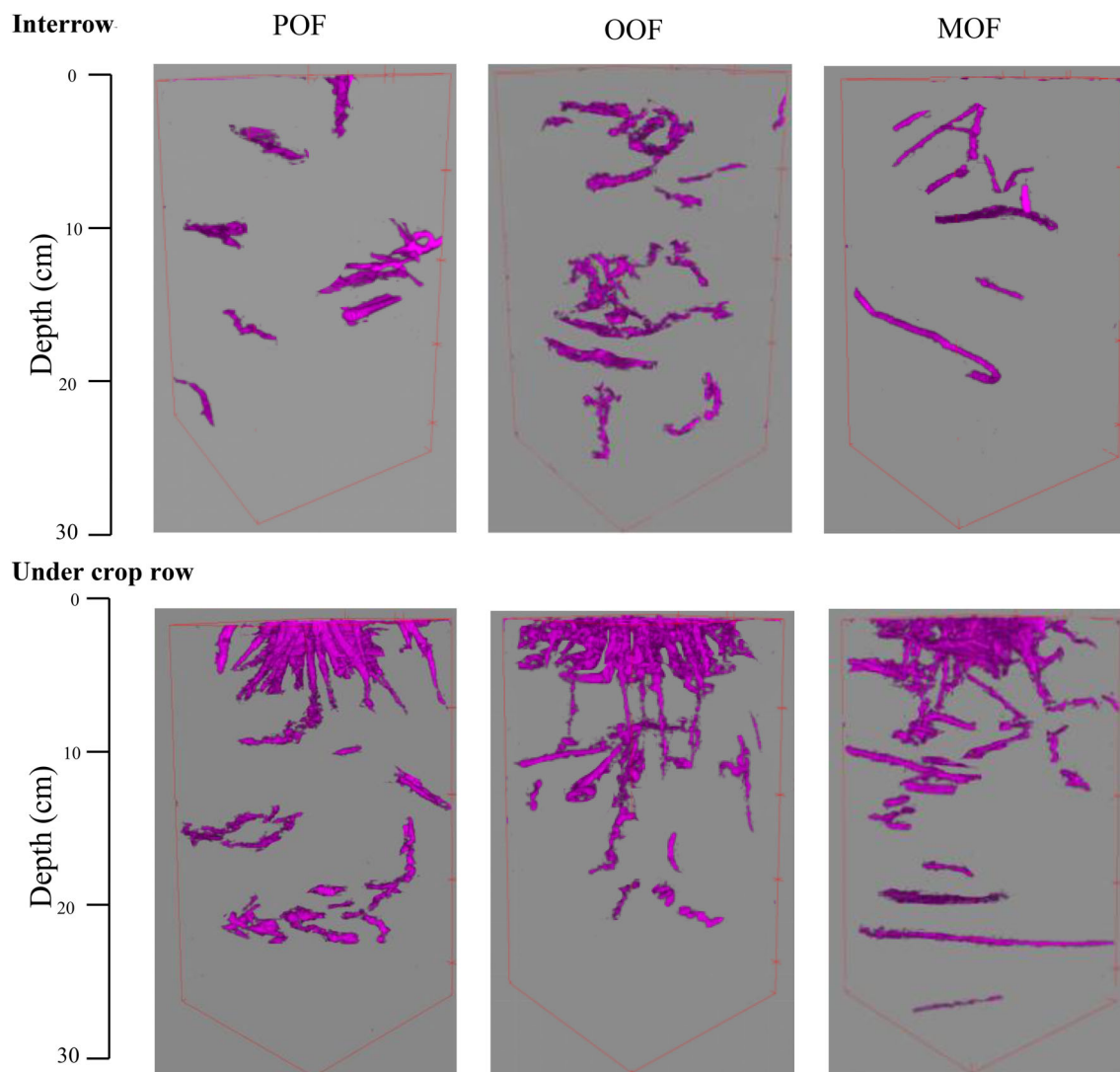


FIGURE 3 Three-dimensional biopore structure in the three types of oasis farmlands. POF is piedmont oasis farmland; OOF is old oasis farmland; MOF is marginal oasis farmland. The dimension of the region of interest is $12\text{ cm} \times 12\text{ cm} \times 27.5\text{ cm}$ for each soil core column. Top: Three-dimensional biopore structure in the interrows of three types of farmlands; bottom: Three-dimensional biopore structure under crop rows of three types of farmlands

TABLE 2 Characteristics of soil macropores across the three types of oasis farmlands as determined by X-ray computed tomography

| | POF | | OOF | | MOF | |
|--|----------|----------|----------|----------|----------|----------|
| | Interrow | Crop row | Interrow | Crop row | Interrow | Crop row |
| Number of macropore | 1153 b | 2876 a | 2270 b | 7660 a | 417 b | 2488 a |
| Macropore volume (mm^3) | 6350 b | 10,719 a | 15,639 | 20,836 | 4026 b | 9956 a |
| Macroporosity (%) | 0.22 | 0.31 | 0.54 | 0.76 | 0.14 b | 0.25 a |
| Bioporosity (%) | 0.09 b | 0.25 a | 0.15 b | 0.53 a | 0.09 b | 0.17 a |
| Total surface area of all macropores (cm^2) | 287 | 322 | 685 | 996 | 156 b | 404 a |
| Fractal dimension | 2.23 | 2.19 | 2.27 | 2.16 | 1.79 | 2.16 |
| Mean macropore diameter (mm) | 3.71 | 3.62 | 3.57 | 3.11 | 4.07 | 3.38 |

Note: Different letters mean significant difference at 0.05 level between crop rows and interrows. The dimension of the region of interest is $12\text{ cm} \times 12\text{ cm} \times 27.5\text{ cm}$ for each soil core column.

Abbreviations: MOF, marginal oasis farmland; OOF, old oasis farmland; POF, piedmont oasis farmland.

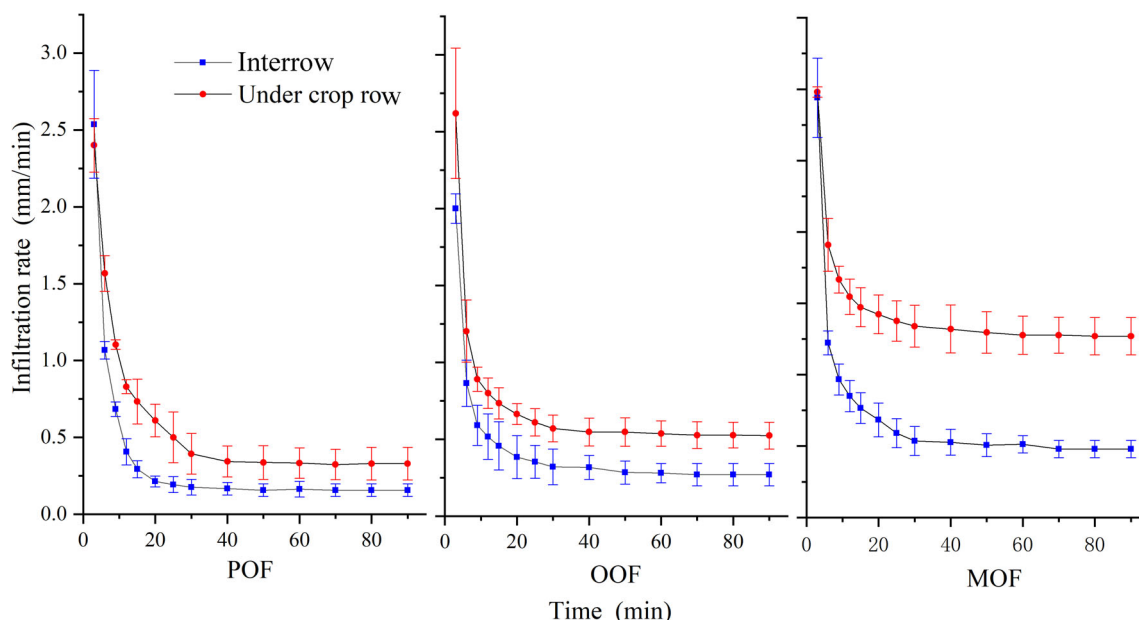


FIGURE 4 Variation of infiltration rate in the three types of oasis farmlands. POF is piedmont oasis farmland; OOF is old oasis farmland; MOF is marginal oasis farmland

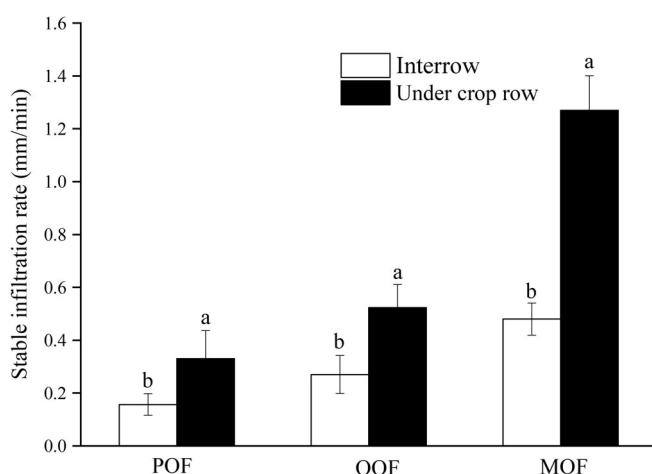


FIGURE 5 Comparison of stable infiltration rate in the three types of oasis farmlands. POF is piedmont oasis farmland; OOF is old oasis farmland; MOF is marginal oasis farmland. Different letters indicate significant difference at 0.05 level between interrows and crop rows

number of macropores was 3.9 times larger under crop rows than interrows across the oasis farmlands. Moreover, bioporosity in soils under crop rows were significantly ($p < 0.05$) larger than interrows (Table 2). The total surface area of all macropores under crop rows was not significant ($p > 0.05$) between interrows and crop rows except at MOF. Meanwhile, there were no significant ($p > 0.05$) differences in fractal dimension and mean

macropore diameter between interrows and crop rows across the oasis farmlands.

3.3 | Soil water infiltration

The infiltration rate varied greatly during the first 6 min and then reached a stable infiltration rate after 30 min (Figure 4). In the infiltration process, the infiltration rates under crop rows were larger than interrows across the oasis farmlands (Figure 4). The average stable infiltration rate in the interrows was less (0.3 mm min^{-1}). However, the average stable infiltration rate under crop rows reached 0.7 mm min^{-1} , indicating that the capacity of soil infiltration affected by crop roots was significantly ($p < 0.05$) enhanced across the oasis farmlands (Figure 5).

3.4 | Characteristics of water flow

Figure 6 shows the binary images of dye-stained soil profiles in the three types of oasis farmlands. The dye coverage decreased with soil depth. The infiltration depth under crop rows was clearly larger than interrows across the oasis farmlands (Figure 6). The uniform infiltration depth in the interrows reached 14.2 cm, while the uniform infiltration depth under the crop rows reached only about 6.3 cm (Table 3). The dye coverage under crop rows was larger than interrows, yet the difference

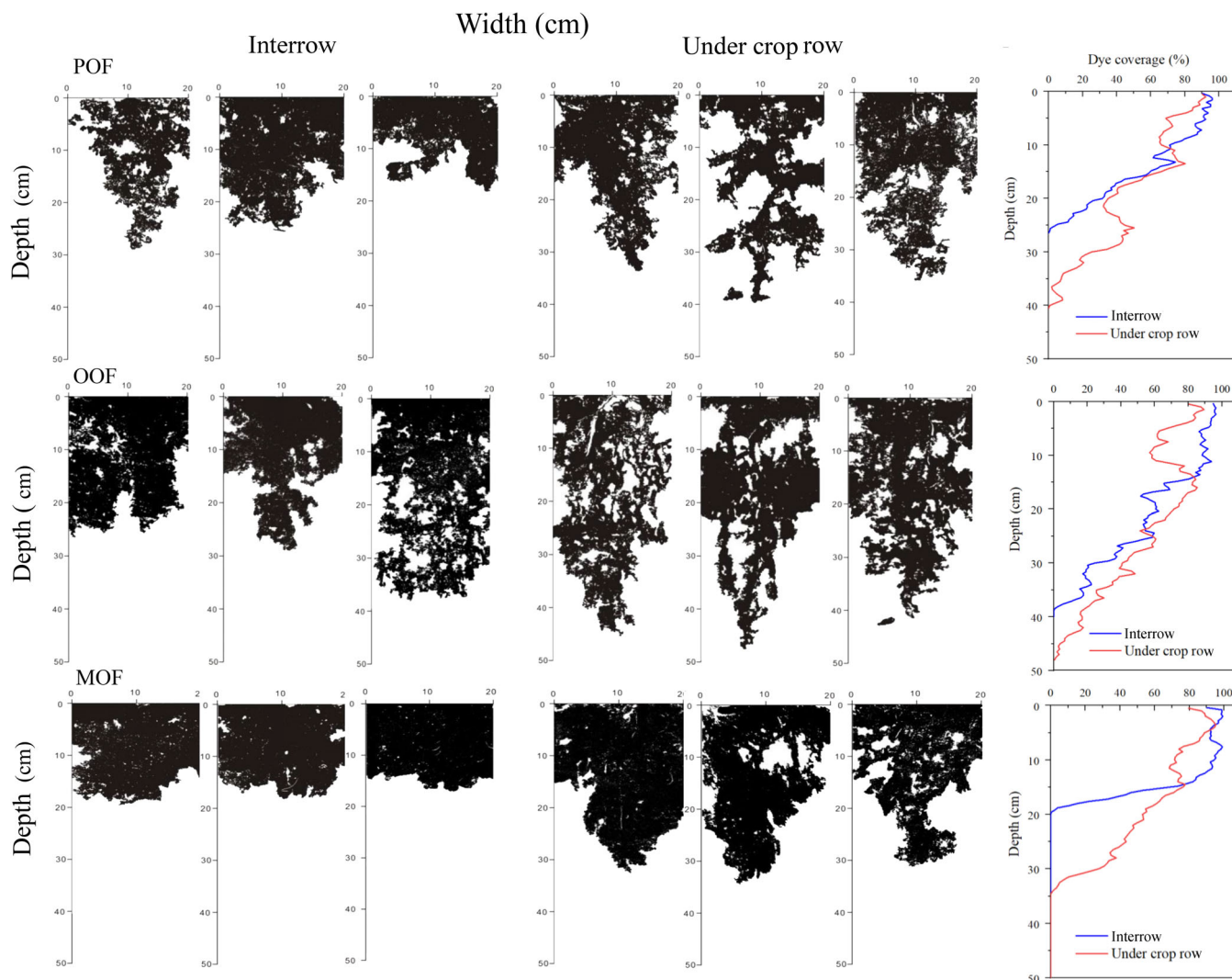


FIGURE 6 Binarized images and examples of dye coverage in soil profiles in the three types of oasis farmlands. Three pictures on the left are interrows, three pictures on the right are under crop rows. POF is piedmont oasis farmland; OOF is old oasis farmland; MOF is marginal oasis farmland

TABLE 3 Dye-stained characteristic parameters in the 0–50 cm soil layer across the three types of oasis farmlands

| | POF | | OOF | | MOF | |
|---------------------------------|--------------|--------------|--------------|--------------|--------------|--------------|
| | Interrow | Crop row | Interrow | Crop row | Interrow | Crop row |
| Dye coverage (%) | 30.2 ± 7.9 | 37.1 ± 2.1 | 45.2 ± 9.1 | 48.1 ± 0.8 | 30.1 ± 1.3 | 39.3 ± 4.7 |
| Uniform infiltration depth (cm) | 12.4 ± 4.7 | 5.2 ± 2.9 | 16.3 ± 3.3 a | 4.8 ± 2.8 b | 14.0 ± 0.4 | 8.8 ± 5.0 |
| Length index | 200 ± 16 b | 299 ± 72 a | 317 ± 98 | 414 ± 28 | 174 ± 25 b | 245 ± 32 a |
| Maximum infiltration depth (cm) | 21.9 ± 4.0 b | 36.3 ± 2.5 a | 33.2 ± 5.0 b | 45.3 ± 2.5 a | 18.4 ± 1.2 b | 32.7 ± 1.3 a |
| Preferential flow fraction (%) | 20 ± 1 b | 72 ± 16 a | 27 ± 13 b | 80 ± 11 a | 7 ± 3 b | 56 ± 21 a |

Note: Values represent means followed by the standard deviation. Different letters mean significant difference at 0.05 level between crop rows and interrows. Abbreviations: MOF, marginal oasis farmland; OOF, old oasis farmland; POF, piedmont oasis farmland.

was not significant ($p > 0.05$; Table 3). Soil water movement in the interrows was dominated by uniform flow (Figure 6).

The average maximum infiltration depths in the interrows of the POF, OOF, and MOF sites were 21.9 cm, 33.2 cm, and 18.4 cm, respectively, while the average maximum infiltration depths under crop rows were 36.3, 45.3, and 32.7 cm, respectively. The maximum infiltration depth under crop rows was 1.6 times larger than interrows, and this difference was significant ($p < 0.05$; Table 3). The length index under crop rows was significantly ($p < 0.05$) larger than interrows except at OOF. The preferential flow fraction under crop rows was 4.8 times larger than interrows across the oasis farmlands. Also, the preferential flow fraction under crop rows was significantly larger than interrows. Preferential flow was obviously observed under crop rows compared to interrows across the oasis farmlands (Figure 6).

4 | DISCUSSION

Plant roots develop root channels and increase soil macropores and porosity (Devitt & Smith, 2002; Lesturgez et al., 2004). Generally, biopores, for example, large root channels, are produced by the root turnover process itself (Rasse et al., 2000). The plant root system could influence the spatial structure of soil pores, for example, macropore length and length density (Li et al., 2019). Our research showed that soil macropores under crop rows were more abundant than interrows across the oasis farmlands. Large root channels and large soil pores constituted most of the pore system under crop rows across the oasis croplands. The volume of the biopores contributed 73% of the volume of the total macropores under crop rows (Table 2). The result is similar to the findings of Zhang, Liu, et al. (2018) who

observed that the volume of the biopores contributed 66%–74% and 30%–58% of the volume of the total macropores in the paddy and upland fields, respectively. The bioporosity in our sites ranged from 0.09% to 0.53% (Table 2), which is compared to the reclamation sites in the Garzweiler open-cast mine (Lucas et al., 2019). The roots channels had a large contribution to the formation of soil macropores (Cheng et al., 2011). The bioporosity under crop rows was 2.7 times larger than interrows across the oasis farmlands. Soil macropores, for example, biopores, were enhanced under the influence of crop roots across the oasis farmlands.

Crop roots have a clearly positive effect on soil water infiltration (Bengough, 2012; Devitt & Smith, 2002). In our study, the stable infiltration rates in soils under crop rows were 2.3 times larger than interrows across the oasis farmlands. It was confirmed that the infiltration rate affected by the root system was larger than the bare soils studied by Bramley et al. (2003). Also, the infiltration rate of soils with *Medicago sativa* roots was larger than under bare soils (Guo et al., 2019). The decomposition and transformation of crop roots can synthesise humus, increase the development of soil aggregates and large pores and decrease bulk density which enhance soil water permeability (Bargués Tobella et al., 2014; Bogner et al., 2008). Water infiltration affected by crop roots was significantly increased compared to the bare soils in the oasis farmlands.

Biopores and large pores created by the crop roots environment directly triggered the occurrence of preferential flow. The characteristics of plant roots are a better predictor of the degree of preferential flow (Zhang et al., 2015). In the oasis farmlands, the maximum infiltration depth in soils under crop rows was larger than interrows. The deeper infiltration under crop rows increased supply of soil water, which was beneficial to the preservation of soil moisture in deep soil layers (Wu et al., 2017). Generally, soil water movement is divided into matrix flow and preferential flow (Hendrickx & Flury, 2001). Water flow mainly

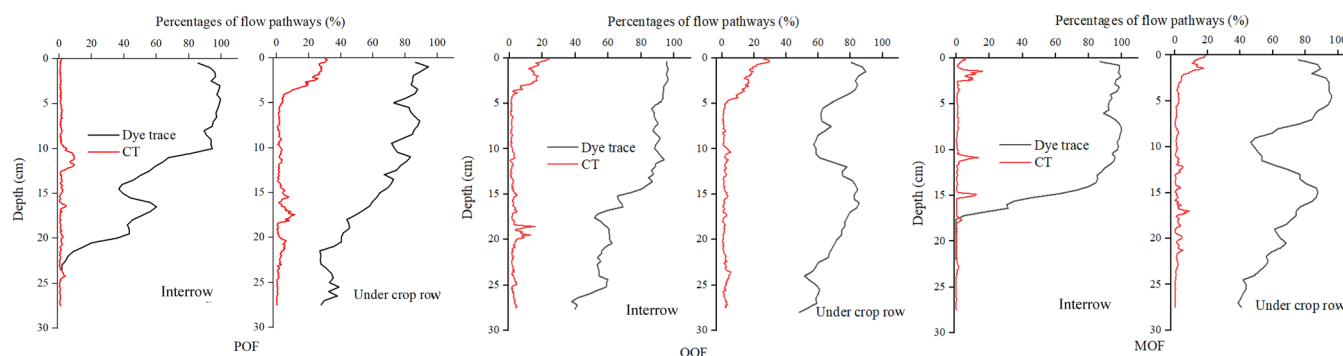


FIGURE 7 Examples of percentages of flow pathways: CT–potential preferential flow in macropores estimated using the X-ray tomography, dye trace–flow in the macropores and soil matrix derived from images of soil dye staining with Brilliant Blue FCF. POF is piedmont oasis farmland; OOF is old oasis farmland; MOF is marginal oasis farmland

TABLE 4 Correlation analysis between soil macropores and water infiltration among the three types of oasis farmlands

| | UID | LI | MID | PFF | Macroporosity |
|---------------|---------|--------|---------|--------|---------------|
| LI | −0.48* | | | | |
| MID | −0.51* | 0.89** | | | |
| PFF | −0.88** | 0.74** | 0.84** | | |
| Macroporosity | −0.39 | 0.68** | 0.72** | 0.57* | |
| NM | −0.59* | 0.62** | 0.750** | 0.71** | 0.85** |

Abbreviations: LI, length index; MID, maximum infiltration depth; NM, number of macropore; PFF, preferential flow fraction; UID, uniform infiltration depth.

*Correlation significant at the 0.05 level (two tailed); Numbers are spearman's correlation coefficients.

**Correlation significant at the 0.01 level (two tailed).

infiltrated in the 0–20 cm layer, but was not able to move to deep soil layer in the interrows. Soil water movement in the interrows was dominated by matrix flow across the oasis croplands. The oasis farmlands were not tilled. Also, soil bulk density between interrows and crop rows did not differ significantly ($p > 0.05$) across the oasis farmlands. Thus, water flow under crop rows was mainly affected by the crop roots, which could move to the lower soil layer after being transported through soil matrix (Figures 6 & 7). Preferential flow dominated water flow process under crop rows across the oasis farmlands. Plant roots had a strong influence in the formation of macropores and their continuity, by extension, and the degree of preferential flow in soil profiles (Zhang et al., 2015). Thus, root channels and large pores provided the main pathways of preferential flow in the crop zone across the oasis farmlands.

The combination of CT and dye tracer enabled us to adequately assess preferential flow through large soil pores in the fields. The methods in quantifying soil macropores and tracing preferential flow has separately attracted attention across different landscapes (Aravena et al., 2011; Bogner et al., 2008). The dye tracer is a destructive method, which could not clearly reveal water flow through large soil pores in the soil profiles (Kodešová et al., 2012). However, CT only visualised soil pores architecture with a static state (Lucas et al., 2019). The implementation of CT alone could not be sufficient to investigate water and solute transport processes (Filipović et al., 2020). In our study, preferential flow indices (LI, MID, and PFF) were positively correlated with the number of macropores and macroporosity ($p < 0.05$; Table 4). It was indicated that soil macropores significantly ($p < 0.05$) influenced preferential flow process in the oasis farmlands using the integration of CT and dye tracer methods. In addition, the dye coverages from soil profile surface down to a depth of about 10–15 cm were close to or more than 80% in both interrows and crop rows, indicating that the dye staining transported in the soil matrix (Figure 7). However, the dye coverage below a depth of about 20–25 cm under crop rows was still observed, but disappeared in the interrows across the oasis farmlands (Figure 6). Preferential flow

occurred with macropores in subsoils studied by Guo et al. (2019). Large pores and biopores were abundantly distributed under crop rows, and the presence of dye staining was detected in the lower soil layer across the oasis farmlands, indicating that staining solution transported in biopores and large soil pores under crop rows. Thus, the integration of CT and dye tracer was a comprehensive approach, which clearly revealed preferential flow through biopores and large pores under crop rows. The oasis soils with biopores and large pores were more likely to produce preferential flow, resulting in soil water moving to deep soil layer in the oasis farmlands.

There are some limitations in assessment of soil macropores and preferential flow across the oasis farmlands in our study. The low resolution of the scanner only allowed to capture macropores with a diameter larger than 0.47 mm. The soil pore system would be better quantified using CT with a higher voxel at soil column scale. Quantifying soil pores requires CT to determine the threshold between the pores and the solid soil phase. An appropriate image threshold is important during image processing because of the subjective perception involved in this step. Some noise (or cracks) under crop rows was present in images using CT (Figure 2). Images interpretation would be challenged but more conducive to accurately capture soil pores in fields. However, the integration of dye tracer and CT clearly revealed preferential flow through biopores and large pores across the oasis farmlands, which are helpful for us to better understand the physical interactions of biopores and large pores on preferential flow and solute transport in hyper-arid regions.

5 | CONCLUSIONS

The crop roots had an important influence on soil macropores and water flow patterns in hyper-arid regions. The crop roots of oasis farmlands increased macropores number of the adjacent soils, and macroporosity was larger. Biopores, for example, large root channels, and large pores were enhanced under the

crop rows. Soil infiltration under crop rows was significantly ($p < 0.05$) increased compared to interrows across the oasis farmlands and corresponding the degree of preferential flow was enhanced affected by crop roots. The integration of dye tracer and X-ray computed tomography is a comprehensive approach, which clearly captures water flow patterns through the soil matrix and macropores in oasis soils with complex pore systems. Preferential flow occurs in the oasis croplands, resulting in soil water and solute moving to deep soil layer. Moreover, when roots can use macropores as pathways to reach deep soil layer, crops benefit from increased uptake of water and nutrients. Our findings have revealed the change of biopores and large pores affected by the crop roots, which further affects water flow patterns across the oasis farmlands.

ACKNOWLEDGEMENTS

This work was supported by the National Natural Science Foundation of China (Nos. 41877153, 42071044) and the Youth Innovation Promotion Association CAS (No. 2020420). We thank the editors and reviewers for their constructive suggestions on this manuscript. We also would like to thank Dr. Adam Roddy at Yale University for his assistance with language and grammatical editing.

AUTHOR CONTRIBUTIONS

Yongyong Zhang: Conceptualization (lead); investigation (lead); methodology (lead); project administration (lead); resources (lead); writing – original draft (lead); writing – review and editing (lead). **Angyuan Jia:** Software (supporting); visualization (supporting). **Wenzhi Zhao:** Supervision (lead). **Jianjun Kang:** Validation (supporting). **Chuan Wang:** Software (equal). **Wenrong Kang:** Visualization (lead). **Zihan Tian:** Software (supporting).

DATA AVAILABILITY STATEMENT

The data used in this paper are available from Yongyong Zhang (zhangyongyong@lzb.ac.cn) upon request.

ORCID

Yongyong Zhang  <https://orcid.org/0000-0002-2084-5647>

REFERENCES

- Aravena, J. E., Berli, M., Ghezzehei, T. A., & Tyler, S. W. (2011). Effects of root-induced compaction on rhizosphere hydraulic properties-X-ray microtomography imaging and numerical simulations. *Environmental Science & Technology*, 45(2), 425–431. <https://doi.org/10.1021/es102566j>
- Backnäs, S., Laine-Kaulio, H., & Kløve, B. (2012). Phosphorus forms and related soil chemistry in preferential flowpaths and the soil matrix of a forested podzolic till soil profile. *Geoderma*, 189, 50–64. <https://doi.org/10.1016/j.geoderma.2012.04.016>
- Bargués Tobella, A., Reese, H., Almaw, A., Bayala, J., Malmer, A., Laudon, H., & Ilstedt, U. (2014). The effect of trees on preferential flow and soil infiltrability in an agroforestry parkland in semiarid Burkina Faso. *Water Resources Research*, 50, 3342–3354. <https://doi.org/10.1002/2013WR015197>
- Benegas, L., Ilstedt, U., Rouspard, O., Jones, J., & Malmer, A. (2014). Effects of trees on infiltrability and preferential flow in two contrasting agroecosystems in Central America. *Agriculture, Ecosystems & Environment*, 183, 185–196. <https://doi.org/10.1016/j.agee.2013.10.027>
- Bengough, A. G. (2012). Water dynamics of the root zone: Rhizosphere biophysics and its control on soil hydrology. *Vadose Zone Journal*, 11(2), vzj2011.0111. <https://doi.org/10.2136/vzj2011.0111>
- Beven, K., & Germann, P. (1982). Macropores and water flow in soils. *Water Resources Research*, 18(5), 1311–1325. <https://doi.org/10.1029/WR018i005p01311>
- Bogner, C., Wolf, B., Schlather, M., & Huwe, B. (2008). Analysing flow patterns from dye tracer experiments in a forest soil using extreme value statistics. *European Journal of Soil Science*, 59(1), 103–113. <https://doi.org/10.1111/j.1365-2389.2007.00974.x>
- Bramley, H., Hutson, J., & Tyerman, S. D. (2003). Floodwater infiltration through root channels on a sodic clay floodplain and the influence on a local tree species *Eucalyptus largiflorens*. *Plant and Soil*, 253, 275–286. <https://doi.org/10.1023/a:1024531325281>
- Cheng, J. H., Zhang, H. J., Wang, W., Zhang, Y. Y., & Chen, Y. Z. (2011). Changes in preferential flow path distribution and its affecting factors in Southwest China. *Soil Science*, 176(12), 652–660. <https://doi.org/10.1097/ss.0b013e31823554ef>
- Davies, B. E. (1974). Loss-on-ignition as an estimate of soil organic matter. *Soil Science Society of America Journal*, 38, 150–151. <https://doi.org/10.2136/sssaj1974.03615995003800010046x>
- Devitt, D. A., & Smith, S. D. (2002). Root channel macropores enhance downward movement of water in a Mojave Desert ecosystem. *Journal of Arid Environments*, 50(1), 99–108. <https://doi.org/10.1006/jare.2001.0853>
- Doube, M., Klosowski, M. M., Arganda-Carreras, I., Cordelières, F. P., Dougherty, R. P., Jackson, J. S., Schmid, B., Hutchinson, J. R., & Shefelbine, S. J. (2010). BoneJ: Free and extensible bone image analysis in ImageJ. *Bone*, 47(6), 1076–1079. <https://doi.org/10.1016/j.bone.2010.08.023>
- Eshel, G., Levy, G. J., Mingelgrin, U., & Singer, M. J. (2004). Critical evaluation of the use of laser diffraction for particle-size distribution analysis. *Soil Science Society of America Journal*, 68(3), 736–743. <https://doi.org/10.2136/sssaj2004.7360>
- Filipović, V., Defterdarović, J., Šimunek, J., Filipović, L., Ondrašek, G., Romić, D., Bogunović, I., Mustaća, I., Čurić, J., & Kodešová, R. (2020). Estimation of vineyard soil structure and preferential flow using dye tracer, X-ray tomography, and numerical simulations. *Geoderma*, 380, 114699. <https://doi.org/10.1016/j.geoderma.2020.114699>
- Frangi, A. F., Niessen, W. J., Vincken, K. L., & Viergever, M. A. (1998). Multiscale vessel enhancement filtering. In W. M. Wells, A. Colchester, & S. Delp (Eds.), *MICCAI 1998. Medical image computing and computer-assisted intervention-MICCAI'98. Lecture notes in computer science* (Vol. 1496). Springer.
- Guo, L., Liu, Y., Wu, G. L., Huang, Z., Cui, Z., Cheng, Z., Zhang, R. Q., Tian, F. P., & He, H. H. (2019). Preferential water flow: Influence of alfalfa (*Medicago sativa* L.) decayed root channels on soil water infiltration. *Journal of Hydrology*, 578, 124019. <https://doi.org/10.1016/j.jhydrol.2019.124019>

- Guo, L., Mount, G. J., Hudson, S., Lin, H., & Levia, D. (2020). Pairing geophysical techniques improves understanding of the near-surface critical zone: Visualization of preferential routing of stemflow along coarse roots. *Geoderma*, 357, 113953. <https://doi.org/10.1016/j.geoderma.2019.113953>
- Heiri, O., André, F. L., & Lemcke, G. (2001). Loss on ignition as a method for estimating organic and carbonate content in sediments: Reproducibility and comparability of results. *Journal of Paleolimnology*, 25(1), 101–110. <https://doi.org/10.1023/A:1008119611481>
- Hendrickx, J. M. H., & Flury, M. (2001). Uniform and preferential flow mechanisms in the vadose zone. In *Workshop on conceptual models of flow and transport in the fractured vadose zone* (pp. 149–187). National Academy Press.
- Jarvis, N. J. (2020). A review of non-equilibrium water flow and solute transport in soil macropores: principles, controlling factors and consequences for water quality. *European Journal of Soil Science*, 71(3), 279–302. <https://doi.org/10.1111/ejss.12973>
- Jiang, X. J., Liu, W. J., Chen, C. F., Liu, J. Q., Yuan, Z. Q., Jin, B. C., & Yu, X. Y. (2018). Effects of three morphometric features of roots on soil water flow behavior in three sites in China. *Geoderma*, 320, 161–171. <https://doi.org/10.1016/j.geoderma.2018.01.035>
- Kang, S. Z., Hao, X. M., Du, T. S., Tong, L., Su, X. L., Lu, H. N., Li, X. L., Huo, Z., Li, S., & Ding, R. (2017). Improving agricultural water productivity to ensure food security in China under changing environment: From research to practice. *Agricultural Water Management*, 179(SI), 5–17. <https://doi.org/10.1016/j.agwat.2016.05.007>
- Kodešová, R., Nêmeček, K., Kodeš, V., & Žigová, A. (2012). Using dye tracer for visualization of preferential flow at macro- and microscales. *Vadose Zone Journal*, 11(1), vzj2011.0088. <https://doi.org/10.2136/vzj2011.0088>
- Koestel, J., & Jorda, H. (2014). What determines the strength of preferential transport in undisturbed soil under steady-state flow? *Geoderma*, 217, 144–160. <https://doi.org/10.1016/j.geoderma.2013.11.0>
- Koestel, J. K., Moeys, J., & Jarvis, N. J. (2012). Meta-analysis of the effects of soil properties, site factors and experimental conditions on solute transport. *Hydrology and Earth System Sciences*, 16(6), 1647–1665. <https://doi.org/10.5194/hess-16-1647-2012>
- Lai, Z., Zhang, Y., Liu, J., Wu, B., Qin, S., & Fa, K. (2016). Fine-root distribution, production, decomposition, and effect on soil organic carbon of three revegetation shrub species in Northwest China. *Forest Ecology and Management*, 359, 381–388. <https://doi.org/10.1016/j.foreco.2015.04.025>
- Lesturgez, G., Poss, R., Hartmann, C., Bourdon, E., Noble, A., & Ratana-Anupap, S. (2004). Roots of *Stylosanthes hamata* create macropores in the compact layer of a sandy soil. *Plant and Soil*, 260(1–2), 101–109. <https://doi.org/10.1023/B:PLSO.0000030184.24866.a>
- Li, X. Y., Hu, X., Zhang, Z. H., Peng, H. Y., Zhang, S. Y., Li, G. Y., Li, L., & Ma, Y. J. (2013). Shrub hydopedology: Preferential water availability to deep soil layer. *Vadose Zone Journal*, 12(4), vzj2013.01.0006. <https://doi.org/10.2136/vzj2013.01.0006>
- Li, Z. C., Hu, X., & Li, X. Y. (2019). Characterization of root architectures and soil macropore networks under different ecosystems using X-ray CT scanning in the Qinghai Lake watershed, NE Qinghai-Tibet plateau. *Journal of Soil Science and Plant Nutrition*, 19(4), 743–757. <https://doi.org/10.1007/s42729-019-00074-3>
- Lipiec, J., Ku, J., Sowińska-Jurkiewicz, A., & Nosalewicz, A. (2006). Soil porosity and water infiltration as influenced by tillage methods. *Soil & Tillage Research*, 89(2), 210–220. <https://doi.org/10.1016/j.still.2005.07.012>
- Liu, Y., Guo, L., Huang, Z., LÁpez-Vicente, M., & Wu, G. L. (2020). Root morphological characteristics and soil water infiltration capacity in semi-arid artificial grassland soils. *Agricultural Water Management*, 235, 106153. [doi:10.1016/j.agwat.2020.106153](https://doi.org/10.1016/j.agwat.2020.106153)
- Lucas, M., Schlüter, S., Vogel, H. J., & Vetterlein, D. (2019). Soil structure formation along an agricultural chronosequence. *Geoderma*, 350, 61–72. <https://doi.org/10.1016/j.geoderma.2019.04.041>
- Luo, L. F., Lin, H., & Li, S. C. (2010). Quantification of 3-D soil macropore networks in different soil types and land uses using computed tomography. *Journal of Hydrology*, 393(1–2), 53–64. <https://doi.org/10.1016/j.jhydrol.2010.03.031>
- Mooney, S. J., & Morris, C. (2008). Morphological approach to understanding preferential flow using image analysis with dye tracers and X-ray computed tomography. *Catena*, 73(2), 204–211. <https://doi.org/10.1016/j.catena.2007.09.003>
- Nimmo, J. R. (2021). The processes of preferential flow in the unsaturated zone. *Soil Science Society of America Journal*, 85(1), 1–27. <https://doi.org/10.1002/saj2.20143>
- Noguchi, S., Tsuboyama, Y., Sidle, R. C., & Hosoda, I. (1997). Spatially distributed morphological characteristics of macropores in forest soils of Hitachi Ohta experimental watershed, Japan. *Journal of Forest Research*, 2, 207–215. <https://doi.org/10.1007/BF02348317>
- Rasse, D. P., Smucker, A. J., & Santos, D. (2000). Alfalfa root and shoot mulching effects on soil hydraulic properties and aggregation. *Soil Science Society of America Journal*, 64(2), 725–731. <https://doi.org/10.2136/sssaj2000.642725x>
- Schindelin, J., Arganda-Carreras, I., Frise, E., Kaynig, V., Longair, M., Pietzsch, T., Preibisch, S., Rueden, C., Saalfeld, S., Schmid, B., Tinevez, J., White, D., Hartenstein, V., Eliceiri, K., Tomancak P., & Cardona, A. (2012). Fiji: An open-source platform for biological-image analysis. *Nature Methods*, 9(7), 676–682. <https://doi.org/10.1038/nmeth.2019>
- van Schaik, N. L. M. B. (2009). Spatial variability of infiltration patterns related to site characteristics in a semi-arid watershed. *Catena*, 78(1), 36–47. <https://doi.org/10.1016/j.catena.2009.02.017>
- Wang, X. P., Cui, Y., Pan, Y. X., Li, X. R., Yu, Z., & Young, M. H. (2008). Effects of rainfall characteristics on infiltration and redistribution patterns in revegetation-stabilized desert ecosystems. *Journal of Hydrology*, 358, 134–143. <https://doi.org/10.1016/j.jhydrol.2008.06.002>
- Wu, J., Liu, W., & Chen, C. (2017). How do plants share water sources in a rubber-tea agroforestry system during the pronounced dry season? *Agriculture Ecosystems & Environment*, 236, 69–77. <https://doi.org/10.1016/j.agee.2016.11.017>
- Zhang, Y., Zhao, W., & Fu, L. (2017). Soil macropore characteristics following conversion of native desert soils to irrigated croplands in a desert-oasis ecotone, Northwest China. *Soil & Tillage Research*, 168, 176–186. <https://doi.org/10.1016/j.still.2017.01.004>
- Zhang, Y. H., Niu, J. Z., Yu, X., Zhu, W., & Du, X. (2015). Effects of fine root length density and root biomass on soil preferential flow in forest ecosystems. *Forest Systems*, 24(1), e012. <https://doi.org/10.5424/fs/2015241-06048>
- Zhang, Y. Y., Zhao, W. Z., He, J. H., & Fu, L. (2018). Soil susceptibility to macropore flow across a desert-oasis ecotone of the

- Hexi corridor, Northwest China. *Water Resources Research*, 54(2), 1281–1294. <https://doi.org/10.1002/2017WR021462>
- Zhang, Y. Y., Zhao, W. Z., Li, X. B., Jia, A. Y., & Kang, W. R. (2021). Contribution of soil macropores to water infiltration across different land use types in a desert–oasis ecoregion. *Land Degradation & Development*, 32, 1751–1760. <https://doi.org/10.1002/ldr.3823>
- Zhang, Y. Y., Zhao, W. Z., Ochsner, T. E., Wyatt, B. M., Liu, H., & Yang, Q. Y. (2019). Estimating deep drainage using deep soil moisture data under young irrigated cropland in a desert-oasis ecotone, Northwest China. *Vadose Zone Journal*, 18, 180189. <https://doi.org/10.2136/vzj2018.10.0189>
- Zhang, Z., Liu, K., Zhou, H., Lin, H., Li, D., & Peng, X. (2018). Three dimensional characteristics of biopores and non-biopores in the

subsoil respond differently to land use and fertilization. *Plant and Soil*, 428(1–2), 453–467. <https://doi.org/10.1007/s11104-018-3689-3>

How to cite this article: Zhang, Y., Jia, A., Zhao, W., Kang, J., Wang, C., Kang, W., & Tian, Z. (2022). Soil macroporosity and water flow in the root zone of oases in hyper-arid regions. *European Journal of Soil Science*, 73(2), e13235. <https://doi.org/10.1111/ejss.13235>